Sidelobe Mitigation in MIMO Radar with Multiple Subcarriers

M. A. Haleem and A. Haimovich
Department of Electrical and Computer Engineering
New Jersey Institute of Technology
Newark, NJ 07102
Email: {haleem, haimovich}@njit.edu

R. Blum
Department of Electrical and Computer Engineeing
Lehigh University
Bethlehem, PA 18015
Email: rblum@lehigh.edu

Abstract—This paper presents the studies on the reduction of peak sidelobe level in distributed MIMO radar with multiple subcarrier signals. Multiple subcarriers with sufficient frequency spacing become an alternative to increasing the number of sensors for sidelobe reduction. It is shown that the multiple subcarrier signals are most effective in reducing sidelobes at locations far from the target. Two signaling methods, namely continuous carrier transmission and Gaussian-OFDM signals are studied with respect to the sidelobe mitigation properties. The paper also presents an upper bound to the peak sidelobe level considering the non-coherent combining. It is shown that with non-coherent combining, the peak sidelobe of the localization metric scales down as $\frac{1}{MNL\sin(3\pi/2L)}$ where L is the number of subcarriers, and M, N are the number of transmit and receive sensors. While there are grating lobes present in the metric with non-coherent combining, there is a grating lobe free region around the mainlobe, lower bounded by $\rho = \pm\frac{Lf_0}{2B}$. With coherent processing, multiple subcarriers are effective in reducing the sidelobes as well as grating lobes.

I. INTRODUCTION

MIMO (multiple-input multiple-output) radar seeks to exploit the ability to illuminate a surveillance volume with multiple waveforms and to jointly process the echoes observed at the sensors [1]-[3]. MIMO radar architectures were suggested with collocated and with distributed antennas [4],[5]. Distributed MIMO radar, which is the focuss of this paper, consists of sensors randomly placed over a large spatial area. In the coherent mode of operation, distributed MIMO radars act as large phased arrays operating in the near-field. As a result, the localization resolution is in the order of the carrier wavelength, far exceeding bandwidth-dependent resolutions of typical radars [2]. In addition to the resolution, the ambiguity arising from the high sidelobe levels has been an issue resulted in significant amount of studies. As we reported in [6], keeping the localization ambiguities under control in distributed MIMO radar requires the use of a number of sensors larger than a threshold. In [7], authors demonstrated techniques to adaptively control the parameters of waveforms transmitted from different polarimetric antennas to mitigate sidelobe ambiguity. Claims were made on the possibility to use the approach, on waveforms transmitted from distributed or collocated elements of MIMO radars. The techniques considered were, control of pulse repetition interval in the case of time separated pulses, and non-linear processing in the case of multiple subcarrier

(OFDM) signals. In this paper, we present an analysis of the performance of a distributed coherent MIMO radar system, which transmits multiple subcarriers from multiple sensors, randomly placed, in a two dimensional plane.

In the analysis presented, we first consider continuous transmission of multiple subcarriers at every sensor. While a typical system would use waveforms modulated over sub-carriers, continuous transmission of subcarriers depicts the worst case scenario on the sidelobe characteristics with respect to waveform design. Further, this initial study simplifies the analytical framework to investigate the effect of multiple subcarriers along with randomly placed sensors on the sidelobe characteristics. Further, using a set of parameters typical of OFDM systems, we demonstrate the capability of multiple subcarriers to mitigate sidelobes.

With a set of ideal waveforms, the autocorrelation of any waveform is an impulse at zero delay, and any pair of waveforms are mutually orthogonal for all delays involved. Such a set of waveforms can eliminate the sidelobes and would lead to a thumbtack shaped *ambiguity function* (AF). Nevertheless, design of waveforms with ideal correlation properties remains a challenge. In this paper we also consider Gaussian-OFDM waveforms, where each subcarrier is subjected to amplitude modulation with a Gaussian pulse. The consideration of Gaussian pulses leads to simplifications in the analysis, while providing an adequate framework to draw conclusions on the sidelobe mitigation capabilities of a system with multiple subcarriers. Also discussed in this paper is the AF of non-coherent processing as a comparison to that of coherent processing. The AF of non-coherent processing serves as an upper bound to that of coherent processing. We derive the AF of non-coherent processing considering a pair of randomly placed transmit and receive sensors and thereby obtain the AF for MIMO radar, operating with multiple subcarriers. This upper bound characterizes the impact of sensor positions and the number of subcarriers.

The remainder of the paper is organized as follows. In the section II to follow, we introduce the model of the MIMO radar system and the signals. In section III, we discuss the ambiguity function of location estimation with continuous subcarriers. Section IV describes the use of Gaussian OFDM waveforms for location and speed estimation. We carry out an

analysis on the non-coherent processing with respect to the use of multiple subcarriers in Section V. The conclusions and acknowledgment are provided respectively in Section VI and Section VII.

II. ANALYTICAL MODEL

The model used here was introduced in [6]. Fig. 1 illustrates main features of the signal model. An analytic signal waveform $\tilde{s}_k(t)$ is transmitted from sensor k, located at the location denoted P, and with polar coordinates (ρ_k, θ_k), where θ_k is measured with respect to an arbitrary horizontal axis. The coordinate system has the origin at an arbitrary point O. Sensors are placed randomly in a cone extending between $-\theta_{max}$ and θ_{max}. In MIMO radar, sensors may transmit distinct signals or the same signal. In the former case, each receiver comprises matched filters to all the transmitted signals. When each sensor transmits a distinct waveform, a localization metric is formed by post-processing at the receivers. Alternatively, all sensors may transmit the same waveform. With suitable phase shifts (or time delays) at each sensor, the energy may be cohered at the desired observation point O. In this case, the processing is divided between the transmitter (phase shifts to cohere the energy) and the receiver (a set of phase shifts applied to the received signals to cohere the energy at the observation point).
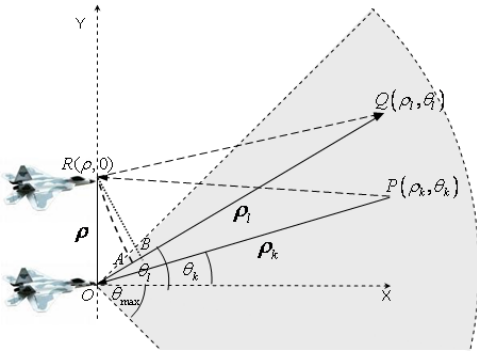

Fig. 1. Illustration of the notation and coordinate system employed in the analysis given in this paper.

Given a MIMO radar system with M transmit and N receive sensors and a target at the origin O, we seek the system response to a point target at location R, specified by its polar coordinates $(\rho, 0)$. The localization is precise if the system is capable of discriminating between targets at O and R. The ability to distinguish between the targets is indicated by the Ambiguity Function. Hence, we seek to formulate the AF for the system as a function of distance ρ and target speed v. With reference to Fig. 1, we are interested in the path differential $\overline{OQ} - \overline{RQ}$ where O is the origin $(0,0)$ and R is $(0, \rho)$. From the figure, we observe that $\overline{OA} = \overline{OQ} - \overline{RQ}$ or $\overline{OA} = \rho_l \left[1 - \sqrt{1 - \left(\frac{2\rho}{\rho_l} \sin\theta - \frac{\rho^2}{\rho_l^2} \right)} \right] \approx \rho \sin\theta_l$. where $\rho_l \gg \rho$ is the distance of sensor l from the origin.

A. Time Delay and Doppler Shift

Using tilde to denote distances, and with c the speed of light, the time delay associated with a target at the origin of the coordinate axes and sensors k and l is

$$\tau_{kl}(O) = \frac{\tilde{\rho}_k + \tilde{\rho}_l}{c}. \tag{1}$$

Denoting the distances normalized to carrier wavelength by ρ, the time delay can be expressed as

$$\tau_{kl}(O) = \frac{\rho_k + \rho_l}{f_0 + f_m} \approx \frac{\rho_k + \rho_l}{f_0}, \tag{2}$$

where f_0 and f_m are respectively the center frequency and the frequency offset corresponding to subcarrier m. The approximation is a result of the fact that $f_0 \gg f_m$ in typical multicarrier systems of interest. Similarly, the time delay associated with a target at R (coordinates $(0, \rho)$) is:

$$\tau_{kl}(R) \approx \frac{\rho_k + \rho_l}{f_0} - \frac{\rho(u_k + u_l)}{f_0}, \tag{3}$$

where $u_k = \sin\theta_k$, and $u_l = \sin\theta_l$. The time differential between the paths $k \to R \to l$ and $k \to O \to l$ is then

$$\mu_{kl} \approx -\frac{\rho(u_k + u_l)}{f_0}. \tag{4}$$

We reflect upon the fact that this model enables us to express differential time delays between sensors as a function of only sensors bearing angles (and not their ranges). This will help to simplify the analysis.

We will further assume that the target at R moves with velocity v along the y axis. Then the signal traveling from the target at R to sensor l experiences a Doppler shift $\frac{(f_0 + f_m)v}{c} u_l$. It is assumed that the Doppler spread due to the signal bandwidth is negligible and thus the Doppler effect is rendered by a simple frequency shift. The Doppler shift along the path $k \to R \to l$ is then given by

$$\phi_{kl} = \frac{(f_0 + f_m)v}{c}(u_k + u_l) \approx \frac{f_0 v}{c}(u_k + u_l). \tag{5}$$

Woodward in [8] expressed the AF in terms of time delay and Doppler shift. Generalized AFs are expressed in terms of time delay, Doppler shift, and angle [9], [10]. In [11], the bistatic radar ambiguity function is expressed in terms of transmitter range, receiver range, transmitter angle, receiver angle, and baseline range. The MIMO radar AF in [12] is expressed as a function of three dimensional vectors of the locations of the transmitters, receivers, target, and a three dimensional vector of velocities. Our model makes simplifying assumptions that enable us to reduce the number of parameters without having to forgo insight. The signal models in [9], [10] are far-field, hence target localization requires range and angle. Our near-field model does not need to measure angles. Finally, vis-a-vis the multistatic cases in [11] and [12], our AFs are dependent only on the sensors bearing angles, a one-dimensional displacement from the origin, and a one-dimensional velocity. But even though our target is restricted to a one-dimensional

space, the two-dimensional sensor deployment supports the target localization and the estimation of its velocity.

B. Signals

Let the signal transmitted from sensor k on subcarrier m in analytic form be,

$$\tilde{s}_{k,m}(t) = s_{k,m}(t)e^{j2\pi(f_0+f_{k,m})t} \qquad (6)$$

for $k = 1, \cdots, M$ and $m = 0, \cdots, L-1$, where $s_{k,m}(t)$ is the complex envelope of the waveform transmitted over subcarrier m. With multiple subcarriers, the signal transmitted from sensor k is a superposition of L signals that can be written as

$$\tilde{s}_k(t) = \sum_{m=0}^{L-1} s_{k,m}(t)e^{j2\pi(f_0+f_{k,m})t}. \qquad (7)$$

In the multiple subcarrier MIMO radar considered in this paper, the same set of subcarriers is used at all the transmitters. The same signal waveform is transmitted from the set of M sensors on the same set of subcarriers. The signals are time and phase adjusted so as to beamform at a location in space. Each receiver performs matched filtering to the transmitted waveform. The outputs of the N receivers are coherently combined to obtain the final output. The time origin, $t = 0$ is taken when the signals reflected from a target at reference point O are time aligned and ready to be processed. Since phase plays an important role, we employ the analytic signal notation. We have for the noiseless analytic signal received at sensor l,

$$\tilde{r}_l^O(t) = M \sum_{m=0}^{L-1} s_m(t)e^{j2\pi(f_0+f_m)t}. \qquad (8)$$

The subscript k in the notation for the signal envelope has been dropped, since the same waveform is transmitted over a subcarrier. After carrier demodulation, the complex envelope is given by

$$r_l^O(t) = M \sum_{m=0}^{L-1} s_m(t). \qquad (9)$$

If a target is found at point R (see Fig. 1), and moving with velocity v, we have

$$\tilde{r}_l^R(t) = \sum_{k=1}^{M} \sum_{n=0}^{L-1} s_n(t-\mu_{kl})e^{j2\pi(f_0+f_n)(t-\mu_{kl})}e^{j2\pi\phi_{kl}(t-\mu_{kl})}, \qquad (10)$$

where the differential delay μ_{kl} and the Doppler shift ϕ_{kl} are defined in (4) and (5) respectively. After carrier demodulation, the complex envelope is given by

$$r_l^R(t) = \sum_{k=1}^{M} \sum_{n=0}^{L-1} s_n(t-\mu_{kl})e^{-j2\pi(f_0+f_n+\phi_{kl})\mu_{kl}+j2\pi\phi_{kl}t}. \qquad (11)$$

In the above (8)-(11), the superscripts O and R distinguish the signals received, respectively from the target at the origin O and R. The ability to resolve between a target at the origin O and a target at point R with polar coordinates $(\rho, 0)$ is measured by the metric:

$$D(\rho, v) = \sum_{l=1}^{N} \int |r_l^O(t) - r_l^R(t)|^2 dt. \qquad (12)$$

Expansion of (12) above results in energy terms constant with respect to ρ and v, and a variable term which is a function of the real part of the function given by

$$\chi(\rho, v) = \sum_{l=1}^{N} \int \left(r_l^O\right)^*(t)r_l^R(t)dt. \qquad (13)$$

Substitution from (9) and (11) in (13) leads to

$$\chi(\rho, v) = M \sum_{k=1}^{M} \sum_{l=1}^{N} \sum_{m=0}^{L-1} \sum_{n=0}^{L-1} \chi_{kl}^{(m,n)}(\rho, v), \qquad (14)$$

where

$$\chi_{kl}^{(m,n)}(\rho, v) = e^{-j2\pi(f_0+f_n+\phi_{kl})\mu_{kl}} \int s_m^*(t) \\ \cdot s_n(t-\mu_{kl})e^{j2\pi\phi_{kl}t}dt. \qquad (15)$$

The magnitude squared term, $\left|\chi_{kl}^{(m,n)}(\rho, v)\right|^2$ of the metric defined in (15) is the AF for a single path between a pair of transmitter and receiver via the target [13]. Accordingly, the magnitude squared term $|\chi(\rho, v)|^2$ of the sum in (14) becomes the composite ambiguity function for the MIMO radar. Desirable ambiguity function achieves the peak when the actual location and speed of the target are equal to the location and speed assumed in the signal combining i.e., when $R \equiv O$ and $v = 0$.

III. LOCATION ESTIMATION WITH CONTINUOUS WAVES

We consider here the case where each of the set of M sensors continuously transmit a set of L subcarriers. Further, the target is assumed stationary such that the Doppler shift $\phi_{kl} = 0$ for all k and l. With the assumption of orthogonality between subcarriers, $\chi_{kl}^{(m,n)}(\rho, v) = 0$ for $m \neq n$. With normalization to achieve a value of unity at $\rho = 0$, the ambiguity function in (14) reduces to

$$\mathcal{A}(\rho) = \frac{1}{MNL} \sum_{k=1}^{M} \sum_{l=1}^{N} \sum_{m=0}^{L-1} e^{j2\pi\left(1+\frac{f_m}{f_0}\right)(u_k+u_l)\rho}. \qquad (16)$$

$\mathcal{A}(\rho)$ is a random function in ρ dependent on the random sensor locations u_k and u_l. From the studies presented in [6], the mean and variance of the sidelobes of $\mathcal{A}(\rho)$ decrease with number of sensors as $\frac{1}{MN}$. Intuitively, the contribution of employing multiple subcarriers to reduce sidelobe levels becomes significant if the changes in phase due to each term are sufficiently large. This implies that $2\pi\frac{f_m}{f_0}(u_k+u_l)\rho \sim \pi$

or equivalently $\frac{f_m}{f_0} \sim \frac{1}{(u_k+u_l)\rho}$. Since typically $\frac{f_m}{f_0} \ll 1$, contributions of subcarrier phase shifts in sidelobe reduction are significant for large ρ. Thus the sidelobes at locations significantly far away from the target can be effectively reduced by the use of multiple subcarriers.

Fig. 2 shows an example of the sidelobe reduction with the use of multiple subcarriers. The parameters used to obtain the results shown are $M = 8$, $N = 8$ sensors and $L = 512$ subcarriers. The 512 subcarriers are assumed to surround a center frequency of $f_0 = 1$GHz and to have a frequency spacing of 78.125kHz thus occupying a bandwidth of 40MHz. Fig. 2(a) shows the AF with a single carrier of frequency f_0 and with fixed equal angular spacing between sensors in the range of $[-45°, 45°]$. In comparison, Fig. 2(b) shows the AF for randomly located sensors where the angular positions of the transmitters are $\theta_k = \{ -33°, -32°, -22°, -22°, 4°, 31°, 35°, 41° \}$ and those of the receivers are $\theta_l = \{ -27°, -23°, -22°, -14°, 2°, 10°, 28°, 39° \}$. Fig. 2(c) is for the case of multiple subcarriers and with positions of sensors as in the case of Fig. 2(b).

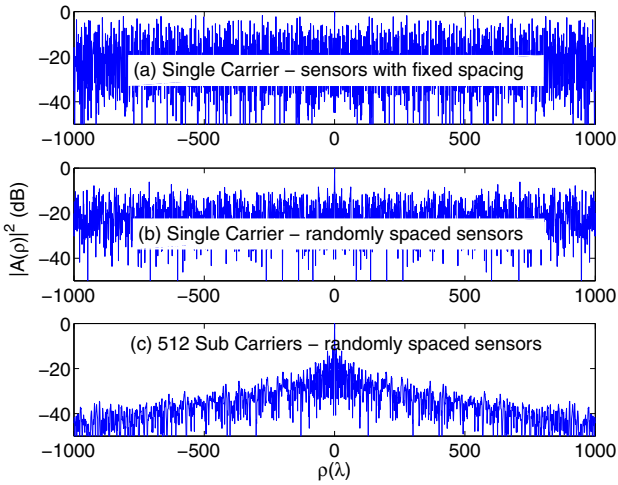

Fig. 2. Example case of sidelobe reduction with multiple subcarriers for 8 transmitters and 8 receivers randomly located in $[-45°, 45°]$ and 512 subcarriers around a center frequency of 1GHz with inter-subcarrier spacing of 78.125kHz.

In comparison with Fig. 2(a) introduced in previous paragraph, a reduction of 10dB is achieved in Fig. 2(b), and it is due to the randomness in sensor locations [6]. The use of multiple subcarriers at the sensors achieves an additional reduction, of up to 40dB in sidelobe levels as seen in Fig. 2(c).

IV. GAUSSIAN OFDM-WAVEFORMS

To illustrate a case of pulsed waveforms transmissions for range and speed estimation, we consider orthogonal or quasi-orthogonal waveforms. Gaussian OFDM waveforms are employed here for this purpose. The signal transmitted on subcarrier m can be expressed

$$u_m(t) = \left(\frac{2}{T^2} \right)^{1/4} e^{-\frac{\pi t^2}{T^2} + j2\pi f_m t}, \qquad (17)$$

where the energy of the pulse is normalized to unity. This pulse is an OFDM subcarrier shaped by a Gaussian pulse. Gaussian-OFDM pulses are quasi orthogonal. In particular, the information carried by each subcarrier can be recovered without significant interference from the other subcarriers if the frequency spacing between the subcarriers is an integer factor of $1/T$, where T is the OFDM pulse duration. Thus we have the subcarrier offset given by $f_m = m/T$. Let there are L subcarriers around the center frequency of f_0. Without loss of generality we assume L is an even number. It can be shown that for the path between transmit sensor k and receive sensor l, the ambiguity function is given by

$$\chi_{kl}(\rho, \upsilon) = e^{-\frac{\pi}{2}\left(\frac{\mu_{kl}^2}{T^2} + \phi_{kl}^2 T^2 \right)} \sum_{m=-L/2}^{L/2-1} \sum_{n=-L/2}^{L/2-1} e^{-\frac{\pi}{2}\left((m-n)^2 \right.}$$
$$\left. +2(m-n)\phi_{kl}T \right) \cdot e^{-j2\pi\left(f_0 + \frac{f_m+f_n+\phi_{kl}}{2} \right)\mu_{kl}}. \qquad (18)$$

Assuming the contribution from terms with $m \neq n$ are negligible, we obtain

$$\chi_{kl}(\rho, \upsilon) \approx e^{-\frac{\pi}{2}\left(\frac{\mu_{kl}^2}{T^2} + \phi_{kl}^2 T^2 \right)} \sum_{m=-L/2}^{L/2-1} e^{-j2\pi\left(f_0 + f_m + \frac{\phi_{kl}}{2} \right)\mu_{kl}}. \qquad (19)$$

Substitution from (4) leads to

$$\chi_{kl}(\rho, \upsilon) \approx e^{-\frac{\pi}{2}\left(\frac{\mu_{kl}^2}{T^2} + \phi_{kl}^2 T^2 \right)} \sum_{m=-L/2}^{L/2-1} e^{j2\pi\left(1 + \frac{f_m}{f_0} + \frac{\phi_{kl}}{2f_0} \right)(u_k+u_l)\rho}. \qquad (20)$$

As discussed in Section 1, delay and Doppler compensation can be performed at transmit sensors such that to beamform at reference point O. In this case, the ambiguity function in normalized form becomes

$$\chi(\rho, \upsilon) = \frac{1}{MNL} \sum_{k=1}^{M} \sum_{l=1}^{N} e^{-\frac{\pi}{2}\left(\frac{\mu_{kl}^2}{T^2} + \phi_{kl}^2 T^2 \right)}$$
$$\cdot \sum_{m=-L/2}^{L/2-1} e^{j2\pi\left(1 + \frac{f_m}{f_0} + \frac{\phi_{kl}}{2f_0} \right)(u_k+u_l)\rho}. \qquad (21)$$

It can be seen in comparison with the case of continuous transmission of subcarriers, in (16), that each term in the summation of Gaussian pulses in (21) is attenuated by a factor less than unity, which results in reduced sidelobe levels. Further, the effect of motion (Doppler) is to decrease or increase the lobe width (helping or hurting localization accurcy) based on whether the Doppler is positive or negative.

Fig. 3 shows an example ambiguity function for the single carrier Gaussian pulse with 4 transmit sensors and

4 receive sensors. The random locations of the sensors are defined by $\theta_k = \{-36°, -16°, 18°, 29°\}$ and $\theta_l = \{-42°, -11°, -6°, 41°\}$. Fig. 4 shows the ambiguity function for a multiple subcarrier system with $L = 64$ with the same sensor placement. The sidelobe reduction with respect to distance (delay) axis is observable. The effect of Doppler is not significant for the typical values of velocity considered.
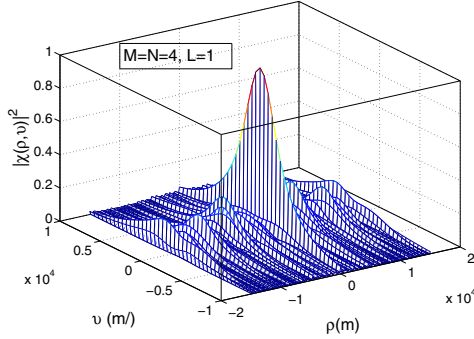

Fig. 3. AF for Gaussian pulse and 4 transmitters, 4 receivers randomly located in $[-45°, 45°]$, $T = 100$ms, and a single carrier of frequency 1GHz.
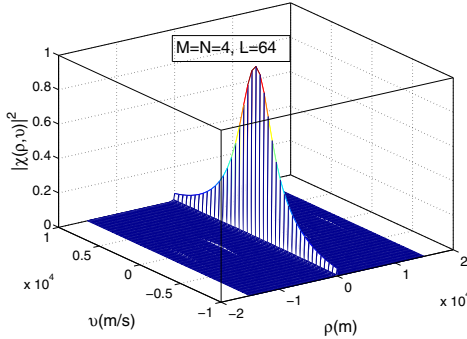

Fig. 4. AF for Gaussian pulse and 4 transmitters, 4 receivers randomly located in $[-45°, 45°]$, $T = 100$ms, and 64 subcarriers around a center frequency of 1GHz with inter-subcarrier spacing of 78.125kHz.

V. COHERENT VERSUS NON-COHERENT PROCESSING

In this section, we carry out an analysis on the non-coherent processing for MIMO radar with multiple subcarriers. This allows us to highlight the effectiveness of multiple subcarriers in the coherent mode, as opposed to non-coherent mode. The ambiguity functions are obtained for the cases of continuous transmission of subcarriers as well as Gaussian-OFDM signals.

Let, the L subcarriers be such that $f_m = m\Delta f$, where Δf is the subcarrier spacing. Thus the signal bandwidth is given by $B = L\Delta f$ The subcarriers are symmetrically placed on either side of a center frequency f_0. Using the identity $\sum_{p=0}^{\beta-1} e^{j\alpha p} = \frac{\sin \frac{\beta\alpha}{2}}{\sin \frac{\alpha}{2}} e^{j(\beta-1)\alpha/2}$ [14], the ambiguity function $A(\rho)$ for continuous wave transmission in (16) can be rewritten as

$$A(\rho) = \frac{1}{MN} \sum_{k=1}^{M} \sum_{l=1}^{N} C(\rho), \qquad (22)$$

where $C(\rho)$ is the AF for a pair of randomly placed transmitter and receiver for the case of continuous waves given by

$$C(\rho) = \frac{\sin \pi \frac{L\Delta f}{f_0}(u_k + u_l)\rho}{L \sin \pi \frac{\Delta f}{f_0}(u_k + u_l)\rho} e^{j2\pi\left(1 - \frac{\Delta f}{2f_0}\right)(u_k+u_l)\rho}. \qquad (23)$$

Compared to the coherent MIMO radar, the AF of the non-coherent MIMO radar can be obtained for the case of continuous subcarrier transmission from (22), and is given by

$$|A(\rho)| = \frac{1}{MN} \sum_{k=1}^{M} \sum_{l=1}^{N} |C(\rho)|, \qquad (24)$$

where $|C(\rho)| = \left| \frac{\sin \pi \frac{L\Delta f}{f_0}(u_k+u_l)\rho}{L \sin \pi \frac{\Delta f}{f_0}(u_k+u_l)\rho} \right|$. The metric in (24) applies to the scenario, where a pair of transmitter and receiver coherently combines the signals on the set of L subcarriers, but the signals for different pairs are combined non-coherently. Similarly, the ambiguity function for non-coherent processing with Gaussian-OFDM signals is obtained from (21), and is given by

$$|A(\rho, v)| = \frac{1}{MN} \sum_{k=1}^{M} \sum_{l=1}^{N} |C(\rho, v)|, \qquad (25)$$

where $|C(\rho, v)| = e^{-\frac{\pi}{2}\left(\frac{\mu_{kl}^2}{T^2} + \frac{\phi_{kl}^2}{T^2}\right)} |C(\rho)|$. The metrics in (24) and (25) can be considered as upper bounds to the AFs of coherent processing respectively for the cases of continuous wave transmission and Gaussian-OFDM signals. Fig. 5 shows an example patterns of $|C(\rho)|$ for continuous wave transmission and $|C(\rho, v)|$ for Gaussian-OFDM waveforms. The mainlobe peaks of $|C(\rho)|$ and $|C(\rho, v)|$ have the value of 1 at $\rho = 0$. The pattern of $|C(\rho)|$ is characterized by grating lobes with peaks at the level of mainlobe peak and a number of sidelobes within the grating lobes. Compared to the case of continuous subcarriers, the Gaussian-OFDM signalling results in reduced grating lobes as expected.

The first sidelobe peak is found at $\rho = \pm\frac{3}{2}\frac{f_0}{B}\frac{1}{(u_k+u_l)}$, and has a value of $\frac{1}{L\sin(3\pi/2L)}$. The subsequent sidelobe peaks occur at $\rho = \pm\left(n + \frac{1}{2}\right)\frac{f_0}{B}\frac{1}{(u_k+u_l)}$ for $n = 1, \cdots, L-2$, and have the values $\frac{1}{L\sin((2n+1)\pi/2L)}$. The sidelobe peak decreases for increasing n until $n = \lfloor L/2 \rfloor$, and subsequently increases for n up to $L-2$. The maximum sidelobe peak is given by the first and last sidelobe peaks within this range. Using the Taylor series expansion for $\sin x$, it can be shown that for large L, the maximum sidelobe peak of $|C(\rho)|$ approaches -13.46dB with respect to the mainlobe peak.

The parameter $(u_k + u_l) \in [0, 2]$ is a random variable. Thus for each path from a transmitter via a target, to a receiver, the positions of sidelobe and grating lobe peaks are random. With M transmit sensors and N receive sensors, there are
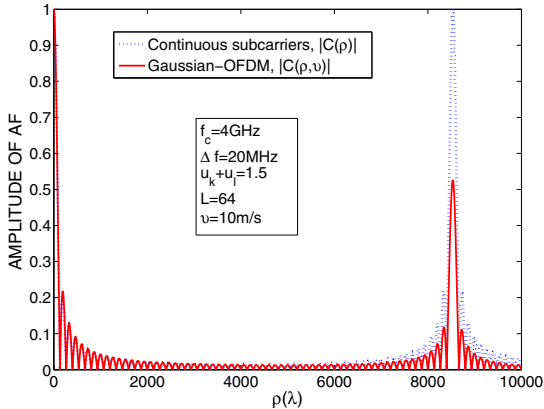
Fig. 5. Example Side lobe and grating lobe patterns for a pair of randomly placed transmitter and receiver with continuous subcarriers and Gaussian-OFDM signals.

MN paths, and all the sidelobe and grating lobe peaks of the AF with non-coherent combining are reduced up to $\frac{1}{MN}$ with respect to the main-lobe peak. With L subcarriers, the maximum sidelobe peak scales down with L as $\frac{1}{L\sin(3\pi/2L)}$ and leads to a peak sidelobe level of $\frac{1}{MNL\sin(3\pi/2L)}$. Further, as shown in the example of Fig. 5, the first grating lobe peak is found at $\rho = \pm\frac{f_0}{\Delta f}\frac{1}{(u_k+u_l)} = \pm\frac{Lf_0}{B}\frac{1}{(u_k+u_l)}$. This implies that for a given carrier frequency, the smaller the value of carrier spacing, the larger the region, free of grating lobes in which we may achieve the -13.46dB sidelobe level with multiple subcarriers. Further, since $(u_k + u_l)$ is upper bounded by 2, the ambiguity free region is lower bounded by $\rho = \pm\frac{Lf_0}{2B}$, and this bound can be increased by increasing L for a given B. Thus the grating lobe free region in the case of non-coherent processing can be controlled by changing L as desired. With coherent processing, the sidelobe as well as the grating lobe peaks are greatly reduced by increasing the number of subcarriers as demonstrated by the simulation results in Section III.

VI. CONCLUSIONS

In this paper, we studied the ambiguity function of range and speed estimation with distributed MIMO radar for multiple subcarrier signals. A simplified two dimensional analytical model was presented, and it was shown to capture all the necessary aspects of the problem. We compared the cases of continuous transmission of multiple subcarriers and Gaussian-OFDM waveforms with respect to the abilities to reduce the sidelobes of the respective ambiguity functions.

With a set of parameters typical of OFDM systems, numerical results were presented showing the effectiveness of multiple subcarriers in reducing the sidelobes. It is seen from the example that while the use of Gaussian-OFDM signals significantly reduces the sidelobe peaks, the radar system still benefits from multiple subcarriers to further reduce the sidelobes. The effect of multiple subcarriers on the accuracy of Doppler estimation however, is not significant.

The advantage of coherent combining of signals with respect to the sensors was highlighted by analyzing non-coherent combining. In this analysis, we obtained metrics for location estimation with continuous subcarriers and location and speed estimation with Gaussian-OFDM waveforms, for a pair of transmit and receive sensors. It was found that the peak sidelobe of these metrics reduces as $\frac{1}{MNL\sin(3\pi/2L)}$ with L subcarriers, M transmit sensors, and N receive sensors. It was also shown that for the non-coherent case, there is a region around the mainlobe peak, free of grating lobes which spans over a range lower bounded by $\rho = \pm\frac{Lf_0}{2B}$. With coherent processing however, sidelobes and grating lobes are significantly reduced by multiple subcarriers.

VII. ACKNOWLEDGMENT

REFERENCES

[1] E. Fishler, A. Haimovich, R. S. Blum, D. Chizhik, L. J. Cimini, and R. A. Valenzuela, "MIMO Radar: An Idea Whose Time Has Come," *Proc. IEEE Radar Conference*, pp. 71-78, April 2004.

[2] N. H. Lehmann, A. M. Haimovich , R.S. Blum, and L. J. Cimini, "High resolution capabilities of MIMO radar," *Proc. of 40th Asilomar Conf. on Signals, Systems and Computers,* Nov. 2006.

[3] Jian Li and P. Stoica, *MIMO Radar Signal Processing*,John Wiley & Sons, Inc., 2009.

[4] Jian Li and P. Stoica, "MIMO Radar with Colocated Antennas," *IEEE Signal Processing Magazine*, vol. 24, No. 5, pp. 106-114, Sept. 2007.

[5] A. Haimovich, R. Blum, and L. Cimini, "MIMO radar with widely separated antennas: Reviewing recent work, *IEEE Sig. Proc. Magazine*, pp. 116-129, January 2008.

[6] M. A. Haleem and A. M. Haimovich, "On the Distribution of Ambiguity levels in MIMO radar," *Proc. of 42nd Asilomar Conf. on Signals, Systems and Computers,* Oct. 2008.

[7] R. Calderbank, S. D. Howard, and B. Moran, "Waveform Diversity in Radar Signal Processing," IEEE Sig. Proc. Magazine," pp. 32-41, Jan. 2009.

[8] P. M. Woodward, *Probability and Information Theory with Application to Radar*. New York: Pergamon, 1957.

[9] H. Urkowitz, C. Hauer, and J. Koval, "Generalized resolution in radar systems," in *Proc. IRE*, Oct. 1962, vol. 50, pp. 2093-2105.

[10] J. V. DiFranco and W. L. Rubin, "Spatial ambiguity and resolution for array antenna systems," *IEEE Trans. on Military Electronics*, July-Oct. 1965.

[11] T. Tsao, M. Slamani, P. Varshney, D. Weiner, and H. Schwarzlander, "Ambiguity function for a bistatic radar," *IEEE Trans. Aerosp. Electron. Syst.*, vol. 33, no. 3, pp. 1041.1050, Jul. 1997.

[12] G. San Antonio, D. F. Fuhrmann, and F. C. Robey, "MIMO radar ambiguity functions," *IEEE Journal on Selected Topics in Signal Processing*, June 2007.

[13] M. I. Skolnik, "Introduction to Radar Systems," Second Edition, Mc-Graw Hill, New York, NY, 2001.

[14] D. R. Wehner, *High Resolution Radar*, 2nd Edition, Artech House Publishers, 1994.